Good coupling for the multiscale patch scheme on systems with microscale heterogeneity

J. E. Bunder* A. J. Roberts† I. G. Kevrekidis‡

June 8, 2016

Abstract

 Computational simulation of microscale detailed systems is frequently only feasible over spatial domains much smaller than the macroscale of interest. The 'equation-free' methodology couples many small patches of microscale computations across space to empower efficient computational simulation over macroscale domains of interest. Motivated by molecular or agent simulations, we analyse the performance of various coupling schemes for patches when the microscale is inherently 'rough'. As a canonical problem in this universality class, we systematically analyse the case of heterogeneous diffusion on a lattice. Computer algebra explores how the dynamics of coupled patches predict the large scale emergent macroscale dynamics of the computational scheme. We determine good design for the coupling of patches by comparing the macroscale predictions from patch dynamics with the emergent macroscale on the entire domain, thus minimising the computational error of the multiscale modelling. The minimal error on the macroscale is obtained when the coupling utilises averaging regions which are between a third and a half of the patch. When the symmetry of the inter-patch coupling matches that of the underlying microscale structure, patch dynamics predicts the desired macroscale dynamics to any specified order of error. The results confirm that the patch scheme is useful for macroscale computational simulation of a range of systems with microscale heterogeneity.

*School of Mathematical Sciences, University of Adelaide, South Australia 5005, Australia. mailto:judith.bunder@adelaide.edu.au

†School of Mathematical Sciences, University of Adelaide, South Australia 5005, Australia. mailto:anthony.roberts@adelaide.edu.au

‡Department of Chemical and Biological Engineering and PACM, Princeton University, Princeton, NJ 08544, USA.

1 Introduction

Across all fields of science and engineering there are many systems which are only realistically described by mathematical models on multiple spatial and temporal scales, where each scale is critical to the model and must be accounted for in any numerical solution [8, 13, 6, e.g.]. Such multiscale systems are notoriously complex and computationally demanding, with computational methods of solution generally requiring enormous reductions in complexity and careful control of errors. One major challenge of multiscale modelling is how to transfer and represent information between different scales, particularly when the different scales are governed by different physics (for example, discrete and continuous, or deterministic and stochastic). A typical scenario is that a macroscale description of the system is required for practical applications, but essential to the system are fine details on microscales which are substantially smaller than the macroscale of interest. One important aim of multiscale modelling schemes is to be sufficiently accurate to reduce the need for expensive and time consuming experiments; for example, in the design of metamaterials with novel properties for new metadevices [35]. This article derives good designs for the computational multiscale modelling scheme of patch dynamics [31, 15, 32, e.g.].

The multiscale computational technique of patch dynamics is 'equation-free' in the sense that it makes no attempt to derive a macroscale closed algebraic model from the original microscale system [11, 15, 20, 17, 32, for reviews]. Numerical resolution of the macroscale dynamics are obtained on demand by computing the microscale system on small discrete patches, with each patch centred about one macroscale grid point. A major advantage of this technique is that it is the original microscale system which is computed, and not an approximation. Unlike many other multiscale modelling techniques [23, 7, e.g.], no assumptions are made regarding the relative importance of the various components of the microscale system since patch dynamics requires no such simplification. Two crucial, previously unresolved, questions in multiscale modelling when applying the patch method to systems with microscale heterogeneity are: (a) how to couple the discrete patches across space so that the unsimulated regions between the patches are best accounted for? and (b) how to appropriately design patches to capture relevant microscale characteristics? This article answers these questions.

A full implementation of patch dynamics involves discretising both space and time [30, 22, 11, 33]. Here we concentrate on the spatial aspects of the patch scheme. Spatial patch dynamics, also known as the gap-tooth scheme, was

successfully applied to various models, including Burgers' equation [25], a generalized advection-diffusion equation [26] and a Ginzburg–Landau model [29], and the resultant macroscale evolution was shown to be effectively independent of both patch width and patch coupling conditions [28]. However, these analyses all invoked systems where the microscale structures are smooth.

Here we explore a discrete, one dimensional, diffusion system, specified in Section 2. In contrast to earlier studies [28, 29, e.g.], we invoke microscale heterogeneity in the diffusion coefficients. We assume that the diffusivity coefficient varies rapidly, with varying periodicity, over the microscale lattice. This diffusion model with fine scale roughness in the diffusivity coefficient generalises previous research into the special case where the diffusion coefficient alternate between two values [2]. The importance of such a discrete microscale diffusion is that it is in the same universality class as a host of other microscale systems. We conjecture that our results apply to a wide variety of microscale systems whose emergent macroscale dynamics are effectively that of diffusive mixing. Consequently, our results describe how to design patch schemes for multiscale modelling of a wide range of problems with microscale heterogeneity.

Multiscale modelling of materials with microscale heterogeneous compositions has broad applications, including the analysis of contact interaction and wear [12], avoiding damage in composite materials [19, 34], modelling of nanostructures [10], and predicting flow in porous media [5]. These problems are often tackled with some spatial averaging or homogenization, but for these techniques the method of solution varies from problem to problem and is typically reliant on heuristic approximations or trial-and-error [21, 16, 14]. Furthermore, their application becomes a daunting tasks when faced with complicated phenomena including nonlinearity [24, 16]. Our aim with patch dynamics is to develop a multiscale modelling method with broad applicability which is straightforwardly adaptable to large families of problems.

Section 2 introduces the patch dynamics scheme and discusses how the microscale heterogeneity complicates the choice of patch size and placement: a patch must capture a sufficient range of diffusivities without giving preference to any diffusivity value. We address these issues with an ensemble average over several configurations of the variable diffusivity coefficient [22]. Section 4 further develops the patch dynamics scheme and presents a method for coupling neighbouring patches and extracting the required macroscale solutions from averages of microscale fields within each patch. Patch dynamics is dependent on several parameters, such as the patch width and how many microscale fields to average over, when calculating the macroscale field. These parameters can be freely chosen: our aim is to determine an optimal choice.

Our results are as yet the only analytic based results for determining optimal patch coupling parameters in a system with microscale heterogeneity. To determine the best choice of parameters we compare the macroscale closure of patch dynamics with that of the microscale solution on the entire microscale domain. Section 3 uses an eigenvalue analysis to analytically derive the macroscale closure over the full microscale domain and Section 5 derives the patch dynamic macroscale closure and details the parameter recommendations for optimum results. We find that it is useful to account for the underlying microscale structure when constructing a patch. When this structure is well known, patch parameters can be chosen to *exactly* reproduce the correct macroscale closure—an ensemble average is unnecessary. However, when the microscale structure is not well known, the ensemble average is useful for better approximating the correct macroscale closure. Section 6 presents numerical simulations which confirm the optimum patch conditions determined from the analysis in Section 5.

For simplicity, we concentrate on diffusion in one dimensional space, but the scheme is adaptable to higher dimensions. Section 4 briefly discusses the two dimensional case. Knapek [18] developed a homogenization-based coarse-graining method for a two dimensional diffusion model with heterogeneous diffusion which showed varying degrees of success. Figure 1(top, mesh) shows a two dimensional simulation of discrete diffusion with fine scale heterogeneity in the diffusion coefficient; the variability in diffusion results in a jagged field across the entire domain. The patch dynamics simulation, indicated by the shaded (coloured) regions in Figure 1, is constructed with six patches in both the x and y directions, providing a total of 36 patches. The patch simulation using a single configuration (top) produces a jagged structure, similar to that of the entire domain solution, but the patch simulation with an ensemble average (bottom) produces a smooth field which interweaves between the jagged entire domain solution. In this simulation we use optimum patch parameters determined from the one dimensional analysis and find that they are also suitable for two dimensions.

Herein we address only linear autonomous dynamics because of the fundamental role of linear systems to nonlinear and/or controlled non-autonomous systems. Firstly, a Hartman–Grobman theorem [1] assures us that generic nonlinear non-autonomous dynamics are topologically equivalent to its linearisation. Secondly, recall that the solutions $\mathbf{u}(t)$ of the nonlinear non-autonomous differential system $\mathrm{d}\mathbf{u}/\mathrm{d}t = \mathcal{L}\mathbf{u} + \mathbf{f}(\mathbf{u}, t)$, $\mathbf{u}(0) = \mathbf{u}_0$, are generally equivalent to the solutions of the integral system $\mathbf{u}(t) = \mathbf{u}_0 + \int_0^t e^{\mathcal{L}(t-s)}\mathbf{f}(\mathbf{u}(s), s)\,\mathrm{d}s$. In the equivalent integral system, the exponential $e^{\mathcal{L}t}$ encodes the solutions of

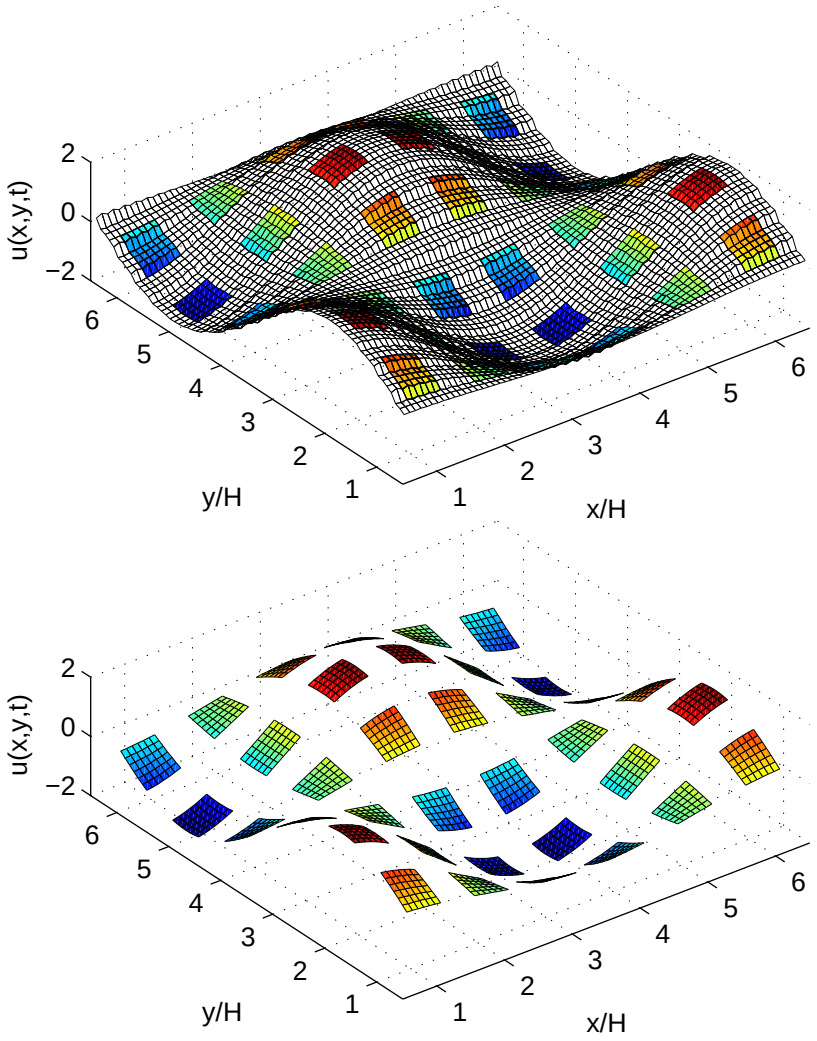

Figure 1: Simulation after time $t = 0.5$ of two dimensional diffusion with diffusivity values which on the microscale are two-periodic in the x direction and four-periodic in the y direction. The black mesh (top) is the entire domain solution, whereas the shaded patches are patch dynamics solutions with (top) one configuration and (bottom) ensemble averaging. Section 4.4 outlines the scheme used.

the linear autonomous $d\mathbf{u}/dt = \mathcal{L}\mathbf{u}$. Thus modelling the linear autonomous dynamics well ($d\mathbf{u}/dt = \mathcal{L}\mathbf{u}$), as explored here, appears to be a necessary prerequisite to good modelling of general nonlinear or non-autonomous dynamics.

2 Microscale heterogeneous diffusion

The canonical microscale problem is discretised diffusion on an infinite, one dimensional, microscale lattice with lattice spacing h,

$$\dot{u}_i(t) = \kappa_i \left[u_{i+1}(t) - u_i(t)\right]/h^2 + \kappa_{i-1}\left[u_{i-1}(t) - u_i(t)\right]/h^2, \qquad (1)$$

where $\dot{u}_i(t)$ is the time derivative of the field $u_i(t)$ at integer lattice point i and $\kappa_i = \kappa_{i \bmod K}$ is the diffusivity coefficient at half lattice point $i + 1/2$. There are $K \geq 2$ independent diffusivity values $(\kappa_1, \kappa_2, \ldots, \kappa_K)$ which repeat periodically on the microscale lattice with period K.

The patch scheme is to simulate the dynamics of the microscale system (1) only within small patches centred on the points of a macroscale grid which itself has large spacing $H \gg h$. We define the macroscale grid points X_j for integer j and define macroscale $U_j(t)$ to be the average of the microscale u_i over a core region around each X_j. This macroscale field $U_j(t)$ is to approximate as best as possible the dynamics of large scale emergent structures of the microscale field $u_i(t)$ governed by the microscale heterogeneous system (1).

As illustrated in Figure 2, we construct small patches of physical width $(2n+1)h$ ($\leq H$) for positive integer patch half-width n, centered about each macroscale lattice point X_j. The patch scheme uses the microscale differential equation (1) for u_i, but only within each patch rather than across the entire domain. To distinguish the fields on the entire domain u_i from the patch dynamics fields over the patches we represent the field in the jth patch by $u_{j,i}$ for $i = 0, \pm 1, \ldots, \pm n$. To obtain a well-posed problem for the patch scheme we must supply appropriate boundary conditions for each patch. These boundary conditions are generally referred to as coupling conditions since their purpose is to couple neighbouring patches by interpolating across the unsimulated space between the patches (see Figure 1). Once coupled, we regard the core averages $U_j(t)$ as forming a macroscale field across the entire domain. Section 4 details the patch construction, coupling conditions and derives the macroscale emergent dynamics.

The heterogenous microscale structure of a system, here specified by the differing diffusivities κ_i, complicates the patch scheme for several reasons. The

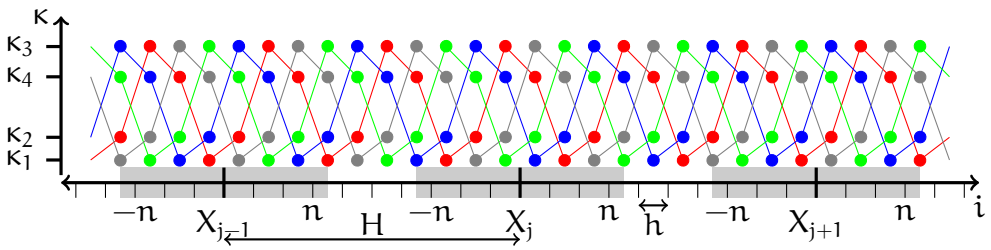

Figure 2: The microscale lattice is indexed by i and indicated by the fine short ticks on the horizontal axis with spacing h. The macroscale lattice is indexed by X_j and indicated by the thick long ticks on the horizontal axis with spacing H. We construct the jth patch of width $(2n+1)h$, here for $n = 3$, about the macroscale lattice point X_j for all j, indicated by the shaded rectangles. Here we represent a microscale system with $K = 4$ specified diffusivity values, $\kappa_1, \kappa_2, \kappa_3, \kappa_4$. The ensemble contains $2K = 8$ configurations: the four shifted configurations are illustrated; the remaining four configurations are reflections of those illustrated.

major issue is whether a patch is big enough to give adequate local averages. Fine scale variations across the microscale lattice produces a microscale field u_i with similar variations, as discernible in the two dimensional simulation of Figure 1(top). Care must be taken to retain important details concerning this microscale structure to avoid compromising the multiscale modelling of the macroscale emergent dynamics. For example, not all diffusivity values will be sampled if patches are smaller than the period of the diffusivities, that is if $(2n+1) < K$, and the patches may destroy shift symmetries inherent in the microscale system (1). Symmetries are destroyed because the microscale system has discrete shift and reflection symmetry across the entire microscale lattice, but with patches of finite size the shift symmetries are often destroyed. When the periodicity of the microscale structure is well known, Section 5.2 shows that with certain patch parameters and only one diffusivity configuration, the emergent dynamics is fully captured to high accuracy. But when the microscale structure is not well known, we must instead analyse an ensemble average of diffusivity configurations, rather than one specific configuration [2].

The ensemble of configurations we invoke contains $2K$ configurations comprising K shifts of the diffusivity values and K reflections of the diffusivity values. The derivation in Section 3 of the large scale emergent dynamics of the system (1) on the entire domain shows that only configurations which preserve the order of the diffusivities are relevant. For periodicity $K = 2$

the shift and reflections coincide. But for $K \geq 3$ the $2K$ configurations are distinct. For example, Figure 2 shows the four shifted configurations for $K = 4$. Figure 1 illustrates the difference between patch dynamics evaluated with a single diffusivity configuration (top) and patch dynamics evaluated with an ensemble average (bottom), with the former retaining the heterogeneous structure of the microscale field and the latter producing a smoothed field. By ensemble averaging, the analysis adequately captures the range of large scale emergent dynamics of the original system (1).

3 Emergent evolution derived on the entire microscale

This section derives the emergent macroscale dynamics of the microscale discrete diffusion system (1), for K-periodic diffusivity values κ_i, over the entire domain. Well established homogenisation gives the leading approximation that the effective macroscale diffusivity is the harmonic mean of κ_i: we both refine this homogenisation and view from a new perspective. Section 5.1 contains a parallel derivation in the case of patch dynamics. A comparison between the emergent dynamics in the two schemes provides a means for measuring the accuracy of the patch dynamics scheme.

Consider dissipative systems of the form $\dot{\mathbf{u}} = M\mathbf{u}/h^2$, such as (1), and the dynamics of macroscale spatial structures characterised by small wavenumber k. Then the long term, emergent dynamics are characterised by the eigenvalue $\lambda_1(k)$, the of matrix M with smallest real-part and its corresponding eigenvector $\boldsymbol{\nu}_1(k)$; that is, the solutions $\mathbf{u} \sim e^{\lambda_1 t/h^2}\boldsymbol{\nu}_1$ after a sufficiently long time t [4, 27]. Figure 3 plots the spectrum of the system (1) for microscale periodicity $K = 4$ against the macroscale wavenumber hk; the top branch is λ_1 which dominates the long term dynamics. Furthermore, in systems with diffusion as the emergent macroscale, the small wavenumber hk (long wavelength) modes decay most slowly across space and thus approximate the macroscale field $U(x,t)$ which is a smooth interpolation of the local core-averaged values $U_j(t)$ (§4.2 makes this more precise) [27]. The long term, emergent macroscale dynamics must therefore evolve at a rate given by the leading eigenvalue λ_1, namely $\dot{U} = \lambda_1 U/h^2$ (in a sense clarified by (9)). This section constructs an analytic expression of this macroscale emergent evolution, which Section 5 compares with the evolution obtained from patch dynamics in order to establish the accuracy of the patch scheme and to determine good patch design.

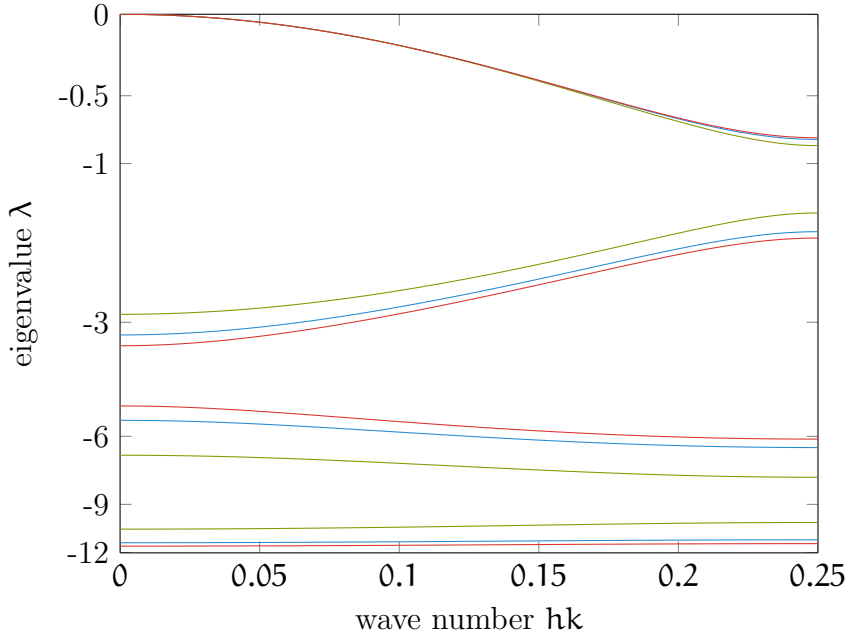

Figure 3: Eigenvalues as a function of wavenumber for a four-periodic microscale $K = 4$ and all possible configurations of diffusivities $\kappa \propto (1, 2, 3, 4)$. There are only three unique sets of eigenvalues since the $2K = 8$ shifts and reflections of one diffusivity configuration give identical eigenvalues. Eigenvalues in the same set are plotted in the same colour (red, blue or green). Our analysis concentrates on the top branch which is almost invariant to the three plotted configurations and characterises the long term, emergent, dynamics of the microscale system. Note that the scaling of the vertical axis is nonlinear.

To determine the eigenspectra of system (1) we partition an effectively infinite domain into cells covering one period of the diffusivity (each cell of length Kh), and then consider the dynamics within each cell but coupled to neighbouring cells. Over the entire domain, the system (1) is then written in operator-matrix-vector form as

$$\dot{\mathbf{u}} = M\mathbf{u}/h^2, \tag{2}$$

for the K dimensional field vector $\mathbf{u}(t) = (u_i, u_{i+1}, \ldots, u_{i-1+K})$ and where the

$K \times K$ operator matrix

$$M = \begin{bmatrix} -\kappa_K - \kappa_1 & \kappa_1 & 0 & \cdots & 0 & \kappa_K \varepsilon^{-K} \\ \kappa_1 & -\kappa_1 - \kappa_2 & \kappa_2 & 0 & \cdots & 0 \\ 0 & \kappa_2 & -\kappa_2 - \kappa_3 & \ddots & \ddots & \vdots \\ \vdots & 0 & \ddots & \ddots & \ddots & 0 \\ 0 & \vdots & \ddots & \ddots & \ddots & \kappa_{K-1} \\ \kappa_K \varepsilon^K & 0 & \cdots & 0 & \kappa_{K-1} & -\kappa_{K-1} - \kappa_K \end{bmatrix}.$$

This matrix introduces the operator ε which is defined to be a microscale shift by one microscale lattice spacing h; that is, $\varepsilon u_i = u_{i+1}$ and its inverse $\varepsilon^{-1} u_i = u_{i-1}$. Consequently, $\varepsilon^{\pm K}$ in the matrix is the shift operator from one K-periodic cell to the next cell to the right/left: it is this operator that couples each cell to its neighbours and hence encodes the system interactions over the infinite domain. With this microscale shift operator ε we transform the original system (1) in an infinite lattice of algebraic variables u_i to the problem (2) in just K operator variables. The shift operator implicitly caters for the infinite lattice.

The dynamics of the matrix form of the microscale system is characterised by the K operator-eigenvalues of the $K \times K$ matrix M (Figure 3 illustrates the $K = 4$ main branches of eigenvalues in one example). These operator-eigenvalues λ satisfy the Kth order characteristic equation

$$c_0(\boldsymbol{\kappa}) + c_1(\boldsymbol{\kappa})\lambda + c_2(\boldsymbol{\kappa})\lambda^2 + \cdots + c_{K-1}(\boldsymbol{\kappa})\lambda^{K-1} + \lambda^K = 0\,, \tag{3}$$

for coefficients c_q which depend upon the diffusivities $\boldsymbol{\kappa} = (\kappa_1, \ldots, \kappa_K)$. We have derived that the coefficients in the characteristic equation (3) are

$$c_0(\boldsymbol{\kappa}) = -\left(\varepsilon^{K/2} - \varepsilon^{-K/2}\right)^2 \kappa_g^K\,, \tag{4a}$$

$$c_q(\boldsymbol{\kappa}) = \frac{\kappa_g^K}{q} \sum_{m_1=1}^{K} \sum_{m_2=1}^{(K-q+1)} \sum_{m_3=1}^{(K-q+2-m_2)} \cdots \sum_{m_q=1}^{(K-1-m_2-\cdots-m_{q-1})} \frac{m_2 \cdots m_q (K - m_2 - \cdots - m_q)}{\kappa_{m_1} \kappa_{m_1+m_2} \cdots \kappa_{m_1+m_2+\cdots+m_q}}\,, \tag{4b}$$

for $1 \le q \le K$. For example, the linear coefficient $c_1 = K^2 \kappa_g^K / \kappa$ where

$$\kappa_g = \left(\prod_{i=1}^{K} \kappa_i\right)^{1/K} \quad \text{and} \quad \kappa = K \left(\sum_{i=1}^{K} \frac{1}{\kappa_i}\right)^{-1} \tag{5}$$

are the geometric and harmonic means of the diffusivities, respectively. Fortunately, we need only to approximately solve the characteristic equation (3) to obtain the leading branch of eigenvalues (at the top of Figure 3).

To describe the emergent macroscale dynamics we only require the smallest magnitude operator-eigenvalue λ_1 with large wavelength (or small wavenumber hk, as shown in Figure 3). As $\|\lambda_1\| \ll 1$ in the regime of interest of small hk, it is sufficiently accurate to approximate the characteristic equation (3) by its quadratic truncation (which is exact for $K = 2$ periodicity), namely

$$c_0(\kappa) + c_1(\kappa)\lambda_1 + c_2(\kappa)\lambda_1^2 \approx 0\,, \quad c_2(\kappa) = \frac{\kappa_g^K}{2} \sum_{m_1=1}^{K} \sum_{m_2=1}^{K-1} \frac{m_2(K-m_2)}{\kappa_{m_1}\kappa_{m_1+m_2}}\,. \tag{6}$$

Unlike the linear coefficient c_1 and the constant coefficient c_0, the quadratic coefficient c_2 is generally dependent on the order of the diffusivities on the microscale lattice. For example, for periodicity $K = 4$

$$c_2(\kappa) = 3(\kappa_1\kappa_2 + \kappa_2\kappa_3 + \kappa_3\kappa_4 + \kappa_4\kappa_1) + 4(\kappa_1\kappa_3 + \kappa_2\kappa_4) \tag{7}$$

is different for configurations of the diffusivities which are not shifts or reflections of each other: for example, $c_2(1,2,3,4) = c_2(2,3,4,1) = c_2(1,4,3,2) = 116$ whereas $c_2(1,3,2,4) = 119$; Figure 3 shows another example in the triplet splitting of the four main branches of eigenvalues. For this reason, when we require an ensemble of diffusivity configurations we choose configurations which preserve the order of the diffusivities; that is, only shifts and reflections of the original order of diffusivity values in the original microscale system (1). This dependence on the order of the diffusivity values is only relevant for periodicity $K \geq 4$ since for periodicities $K = 2$ and 3 all configurations are reflections or shifts of each other. The dependence of c_2 on the ordering of diffusivity values shows that in principle the detailed microscale structure of the system (1) does affect the dynamics on the macroscale, albeit almost unnoticeable for the interesting leading branch in Figure 3. Section 5 shows that the patch scheme is able to account for different permutations of the microscale structure.

For the quadratic approximation (6) of the characteristic equation (3), the smallest magnitude operator-eigenvalue

$$\lambda_1 = -\frac{K^2\kappa_g^K}{2\kappa c_2(\kappa)}\left[1 - \sqrt{1 + 4\kappa c_2(\kappa)\left(\varepsilon^{K/2} - \varepsilon^{-K/2}\right)^2/K^2}\right]. \tag{8}$$

Hence the macroscale emergent evolution

$$\begin{aligned}\dot{U} &= \lambda_1 U/h^2 \\ &= -\frac{K^2\kappa_g^K}{2h^2\kappa c_2(\kappa)}\left[1 - \sqrt{1 + 4\kappa c_2(\kappa)\left(\varepsilon^{K/2} - \varepsilon^{-K/2}\right)^2/K^2}\right] U\end{aligned}$$

$$= \frac{\kappa}{h^2}\left[\delta^2 + \left(\frac{K^2-1}{12} - \frac{c_2(\kappa)\kappa^2}{K^2\kappa_g^K}\right)\delta^4\right] U + \mathcal{O}(\delta^6 U)\,, \tag{9}$$

in terms of the microscale centred difference operator $\delta = \varepsilon^{1/2} - \varepsilon^{-1/2}$. The expansion of the square root uses the operator identity

$$\left(\varepsilon^{K/2} - \varepsilon^{-K/2}\right)^2 = K^2\left[\delta^2 + (K^2-1)/12\,\delta^4\right] + \mathcal{O}(\delta^6),$$

where we expand the square root to error $\mathcal{O}(\delta^6)$ since this corresponds to the error $\mathcal{O}(\lambda_1^3)$ in the quadratic (6). The macroscale evolution (9) treats the difference operator δ as small because $\delta^2 U = (\varepsilon + \varepsilon^{-1} - 2)U$ measures a change over a microscale of the slowly varying macroscale solution U, and this variation must be small for slowly varying fields (small wavenumbers hk in Figure 3); that is, $\delta^2 U \ll U$.

3.1 Approximate to limit combinatorial explosion

Section 5 aims to use equation (9) to determine good parameters for high accuracy modelling by the patch scheme. But with the extra design parameters of the patch scheme, the combinatorial explosion of general possibilities is far too restrictive, even for computer algebra, particularly when requiring an ensemble average with large K. To analytically explore a reasonable range of parameters we mostly only consider the leading λ_1 for moderate heterogeneity.

To compare the emergent leading λ_1 for moderate variations in diffusivities we set $\kappa_i = \kappa_0(1+\eta_i)$ for some fixed reference diffusivity κ_0 and dimensionless relative variation η_i: we analyse the regime where the variations in η_i are big enough that quadratic effects are significant, but small enough that cubic effects are negligible. In terms of the relative variations in the diffusivities, $(\eta_1,\ldots,\eta_K)$, the macroscale, entire domain, evolution is of the form $\dot{U}_j = \lambda_1 U_j/h^2$ where, from equation (9),

$$\begin{aligned}\lambda_1 = \frac{\kappa_0}{h^2}&\left(1 + d\sum_{i=1}^{K}\eta_i - d_0\sum_{i=1}^{K}\eta_i^2 + \sum_{i=1}^{K}\sum_{k=1}^{K/2} d_k\eta_i\eta_{i+k}\right)\delta^2 \\ &+ \frac{\kappa_0}{h^2}\left(f_0\sum_{i=1}^{K}\eta_i^2 + \sum_{i=1}^{K}\sum_{k=1}^{K/2} f_k\eta_i\eta_{i+k}\right)\delta^4 + \mathcal{O}(\delta^6,\eta^3),\end{aligned} \tag{10}$$

where $\eta = |(\eta_1,\ldots,\eta_K)|$. In the expansion (10), the linear coefficient $d = 1/K$, and

$$d_0 = \frac{K-1}{K^2}\,,\quad d_k = \frac{2}{K^2} \text{ for } k \neq 0, K/2\,,\quad d_{K/2} = \frac{1}{K^2}\,,\quad f_0 = \frac{K^2-1}{12K^2}\,,$$

$$f_k = \frac{1}{K^2}\left[\frac{K^2-1}{6} - k(K-k)\right] \text{ for } k \neq 0, K/2\,, \quad f_{K/2} = -\frac{K^2+2}{24K^2}\,. \qquad (11)$$

Section 5 mostly uses these coefficients to assess the accuracy of the emergent dynamics of the various patch schemes. For example, we use the relative error in the d_k coefficients (24) to assesses the accuracy of the patch scheme as K, n and other parameters are varied.

4 Specify the patch scheme

We now turn to the analysis of the scheme where the microscale system (1) is only computed on small distributed patches across space (e.g., Figure 1(bottom) in 2D). Section 4.1 details the patch design and discusses issues particular to systems with microscale heterogeneity, such as the diffusion system (1) or agent/particle based simulators. Section 4.2 discusses our method for obtaining the emergent macroscale dynamics of the patch scheme, and Section 4.3 defines the patch coupling conditions. The test of a patch scheme is simply how well it describes known emergent dynamics. Section 5 shows that our scheme does effectively reproduce the known emergent dynamics of the original microscale system (1) (derived in Section 3) when we choose good parameters in the design.

4.1 Patch construction

As indicated in Figure 2, let the jth patch be of width $(2n+1)h$, for integer patch half-width n and microscale lattice spacing h, and centred on the macroscale lattice point X_j. Our imposition of patches may introduce some unphysical features into the macroscale dynamics. For example, if the patches are positioned such that diffusivity κ_1 always appears on the left edge of each patch, this gives κ_1 a significance which does not exist in the original system. Also, within a patch some diffusivity values may appear more often than others, which again gives greater significance to some microscale features over others. These issues are due to the patches destroying some shift symmetries of the original system (1). For example, unphysical drift terms may appear in the macroscale if the patch design is not good enough.

Sometimes we are able to apply good patch parameters which maintain the correct symmetry (Section 5), but when we cannot do this, the symmetry is restored by analysing an average over an ensemble of shifted and reflected

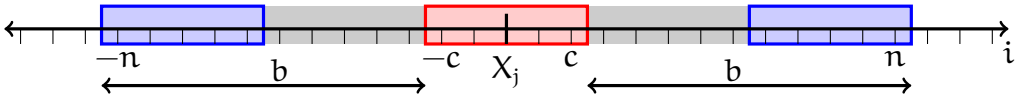

Figure 4: One patch, similar to those shown in Figure 2, but with patch half-width $n = 12$ and action and core half-widths $c = 2$. The outlined region in the centre of the patch, $|i| \le c$, is the core used for the amplitude (13). The two outlined regions on the ends of the patch, $(n - 2c) \le |i| \le n$, are the action regions used for the coupling conditions (15). The so-called buffers are the regions from the edges of the patch to the edges of the core and both buffers have width $b = n - c$.

diffusivity configurations [22]. This ensures that all diffusivities are treated equally and the modelling is independent of how the patches are positioned on the entire domain. We index each of $2K$ configurations by the subscript ℓ, $\kappa_\ell = (\kappa_{1,\ell}, \ldots, \kappa_{K,\ell})$, and the discrete diffusion equation (1) on the jth patch with configuration ℓ is, for $|i| \le (n-1)$ and $\ell = 1, 2, \ldots, 2K$,

$$\dot{u}_{j,i,\ell}(t) = \kappa_{i,\ell}\left[u_{j,i+1,\ell}(t) - u_{j,i,\ell}(t)\right]/h^2 + \kappa_{i-1,\ell}\left[u_{j,i-1,\ell}(t) - u_{j,i,\ell}(t)\right]/h^2 . \quad (12)$$

When we do not require an ensemble average, then we use only one configuration.

Our patch dynamics method is to solve equation (12) for all fields $u_{j,i,\ell}$ in all patches j and for all configurations ℓ (either $\ell = 1$ or $\ell = 1, \ldots, 2K$), with patch coupling conditions defined in Section 4.3. Section 4.4 discusses how the scheme adapts to two dimensions.

4.2 Extracting a macroscale field

Once the ensemble of systems (12) within the jth patch is solved for $u_{j,i,\ell}$ with appropriate coupling conditions, we need to extract a macroscale field from these $u_{j,i,\ell}$. We use a macroscale field—often called an amplitude condition—which is averaged over both the ensemble and the microscale core values $u_{i,j,\ell}$ of the jth patch:

$$U_j(t) = U(X_j, t) = \left\langle \sum_{i=-c}^{c} \frac{u_{j,i,\ell}}{2c+1} \right\rangle , \quad (13)$$

where the angle brackets represent the ensemble average over all configurations ℓ. The integer c, which we call the core half-width, satisfies $0 \le c < n$.

Figure 4 illustrates a patch and highlights the core region. The amplitude condition requires an ensemble average because we only want one macroscale value at each X_j, not a macroscale value for each configuration ℓ.

Some patch dynamics methods do not invoke an average over the patch core and so extract a macroscale value by simply using the microscale solution at the centre of the patch [25, 29, e.g.], corresponding to $c = 0$ in equation (13). However, these methods are typically for systems with smooth microscale structures, resulting in smooth microscale fields which vary only slightly within the patch. Given the heterogeneous microscale structure, which produces a jagged microscale field, an average over the microscale field within the patch core is needed to reduce the influence of the microscale fluctuations.

The patch fields $u_{j,i,\ell}$ outside the core are computed but only indirectly contribute to the macroscale value (13). The purpose of this additional computation is to allow space for the field to evolve from the coupling conditions imposed near the patch edge, thus shielding or 'buffering' the fields within the core and the subsequent macroscale solution. The 'buffer' regions are defined by $c < |i| \leq n$ with buffer width $b := n - c$. Samaey et al. [31] argued that it is possible to define quite arbitrary patch coupling conditions, provided suitably large buffers are chosen. Section 5 considers how the patch and core half-widths, n and c, affect the large scale emergence of the macroscale dynamics, and determines good choices.

4.3 Patch coupling conditions

To solve the patch system (12) for $u_{j,i,\ell}$ within the jth patch for one particular configuration ℓ, we need to specify two coupling conditions to form a well-posed system. An interpolation of the macroscale value U_j and its nearest macroscale neighbours, $U_{j\pm1}$, $U_{j\pm2}$,..., determines the coupling conditions for the jth patch. For smooth microscales, the coupling conditions are only applied to the patch edges $i = \pm n$ [25, 29, e.g.]. However, for heterogeneous microscales, fixing the microscale fields on the patch edges, $u_{j,\pm n,\ell}$, is not practical. The heterogeneous structure of the microscale produces fields $u_{j,i,\ell}$ with a correspondingly jagged structure which tends to be compromised by strict requirements at a single point such as $i = \pm n$. Therefore, analogous to the amplitude condition (13), the coupling conditions constrain an average over the microscale grid values in the so-called 'action regions' shown in Figure 4.

We specify coupling conditions compatible with the amplitude condition (13)

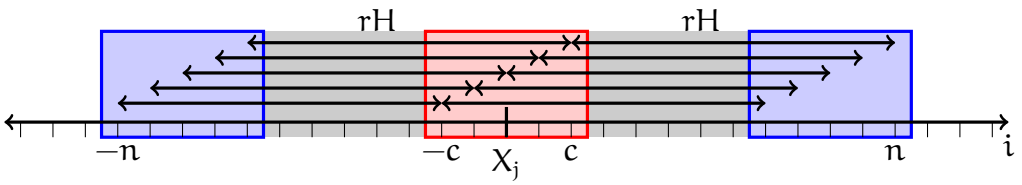

Figure 5: Adding to Figure 4, this figure illustrates shifts of $b = n - c$ microscale steps h, or equivalently, the fraction r of a macroscale step H, from points within the core to corresponding points within the action regions. For some purposes it is useful to identify each point in the action regions as a distance $rH = bh$ from a point in the core.

as then some beautiful results follow, as shown in Section 5.2. The coupling conditions invoke the microscale and macroscale step operators, ε and $\bar{\varepsilon}$, respectively. Section 3 defines the microscale step operator ε to shift the microscale field by one microscale lattice spacing h: the shift ε still operates in the same way for the patch scheme, that is, $\varepsilon^{\pm 1} u_{j,i,\ell} = u_{j,i\pm 1,\ell}$. Crucially, for the field in the jth patch to correspond to the macroscale variations, we must have the shift $\varepsilon^{\pm b}$ of the macroscale value (13) into the right/left action region of the patch matching the average field there:

$$\varepsilon^{\pm b} U_j = \left\langle \sum_{i=n-2c}^{n} \frac{u_{j,\pm i,\ell}}{2c+1} \right\rangle . \tag{14}$$

The two requirements (14) are fundamental expressions of the two coupling conditions.

But to implement the coupling conditions (14) we must convert and approximate them. To express the left-hand side of (14) to be explicit in the macroscale values U_j we define $r := bh/H$ (as illustrated by Figure 5) which is the shift from one grid point in the core to corresponding grid points in the action regions, as a fraction of the macroscale step. We also define the macroscale step operator $\bar{\varepsilon}$ which shifts the macroscale field by one macroscale lattice spacing H: $\bar{\varepsilon}^{\pm} U_j = U_{j\pm 1}$. Thus, in the coupling (14) $\varepsilon^{\pm b} U_j = \bar{\varepsilon}^{\pm r} U_j$. For conciseness, define the macroscale difference and mean operators, $\bar{\delta} := \bar{\varepsilon}^{1/2} - \bar{\varepsilon}^{-1/2}$ and $\bar{\mu} := (\bar{\varepsilon}^{1/2} + \bar{\varepsilon}^{-1/2})/2$, respectively. Then rewrite $\bar{\varepsilon}^{\pm r} U_j$ in terms of $\bar{\mu}$ and $\bar{\delta}$, and expand in powers of $\bar{\delta}^2$, which are small when operating on U_j since the macroscale field U_j varies slowly in space. Thus the coupling conditions (14) correspond to the following which

are defined in terms of averages over action regions:

$$U_j + \sum_{k=1}^{\Gamma} \left(\prod_{l=0}^{k-1} (r^2 - l^2) \right) \gamma^k \frac{\pm(2k/r)\bar{\mu}\bar{\delta}^{2k-1} + \bar{\delta}^{2k}}{(2k)!} U_j + \mathcal{O}(\gamma^{\Gamma+1}) = \sum_{i=n-2c}^{n} \frac{u_{j,\pm i,\ell}}{2c+1}, \tag{15}$$

where Γ is some truncation of the infinite sum in terms of the introduced coupling order parameter γ. The coupling conditions (15) do not have an ensemble average because we need two patch coupling conditions for each configuration ℓ: the conditions (15) are sufficient to ensure (14), albeit approximated by the truncation.

The coupling order parameter γ is an artifice to control the strength of information exchange between patches. It is useful for establishing theoretical support for patch dynamics as detailed in analogous situations elsewhere [26, 28, 32]. We briefly summarise the main points here. For the unphysical case of zero coupling strength, $\gamma = 0$, the patches are isolated from each other and all eigenvalues of the microscale diffusion system on the jth patch have negative real parts except for one zero eigenvalue. Therefore, a slow manifold exists in some finite domain about $\gamma = 0$, global in U_j, and of dimensionality equal to the number of patches. The whole system dynamics is attracted to this slow manifold on a cross-patch diffusion time, and thereafter the system evolves slowly: it is this slow evolution that forms the macroscale dynamics of interest. A power series in coupling γ approximates the slow manifold—this series approximates the leading branch λ_1 of eigenvalues of Figure 3. Although the radius of convergence in γ is generally unknown, we conjecture that evaluation at the physical case of full coupling $\gamma = 1$ is sufficiently accurate to form useful models as it does in other examples [26, 28, e.g.]. The error in the coupling conditions (15) of order $\gamma^{\Gamma+1}$ is equivalent to errors of order $\bar{\delta}^{2(\Gamma+1)}U_j$ and $\bar{\mu}\bar{\delta}^{2\Gamma+1}U_j$, which are small enough provided the macroscale field U_j varies slowly enough across the macroscale spacing H. In essence, this error is the same as analogous familiar error statements in traditional finite difference/element/volume discretisations with spacing H.

The specified coupling conditions (15) invoke two action regions, $n - 2c \leq |i| \leq n$, where the width of each action region equals the core width (as illustrated in Figure 5). It is possible to generalise the action region to some arbitrary half-width a with $0 \leq a < n$ by simply replacing all incidences of 'c' with 'a' in the coupling conditions (15). Preliminary work for the diffusive system (12) suggested that better results are generally obtained when the action and core widths are equal as invoked here.

The coupling conditions (15) are defined in terms of the macroscale mean and difference operators $\bar{\mu}$ and $\bar{\delta}$, whereas the emergent evolution (9) on the entire domain is expressed in terms of the microscale operator δ. To compare the dynamics of the patch scheme with that on the entire domain we must convert expressions from one form to the other. Now write the macroscale second difference operator $\bar{\delta}^2 = \bar{\varepsilon} + \bar{\varepsilon}^{-1} - 2$ and then substitute $\bar{\varepsilon}^{\pm 1} = \varepsilon^{\pm b/r}$ in terms of the microscale shift ε. Substitute $\varepsilon^{\pm 1} = 1 \pm \mu\delta + \delta^2/2$, where the microscale mean operator $\mu := (\varepsilon^{1/2} + \varepsilon^{-1/2})/2$, and on performing a binomial expansion in 'small' differences $(\pm\mu\delta + \delta^2/2)$,

$$\begin{aligned} \bar{\delta}^2 &= (1 + \mu\delta + \delta^2/2)^{b/r} + (1 - \mu\delta + \delta^2/2)^{b/r} - 2 \\ &= \sum_{l=1}^{\infty} C_l^{b/r} \left[(\mu\delta + \delta^2/2)^l + (-\mu\delta + \delta^2/2)^l \right], \end{aligned} \tag{16}$$

where the combinatorial coefficient $C_p^q := \Gamma(q+1)/\left[\Gamma(p+1)\Gamma(q-p+1)\right]$. A similar derivation gives the inverse relationship, from microscale δ^2 to macroscale $\bar{\delta}$ and $\bar{\mu}$, namely

$$\delta^2 = \sum_{l=1}^{\infty} C_l^{r/b} \left[(\bar{\mu}\bar{\delta} + \bar{\delta}^2/2)^l + (-\bar{\mu}\bar{\delta} + \bar{\delta}^2/2)^l \right]. \tag{17}$$

The conversion of $\bar{\mu}\bar{\delta}$ into microscale operators is also useful. Following a similar derivation as above, but with $\bar{\mu}\bar{\delta} = (\bar{\varepsilon} - \bar{\varepsilon}^{-1})/2$, determines

$$\begin{aligned} \bar{\mu}\bar{\delta} &= \sum_{l=1}^{\infty} \tfrac{1}{2} C_l^{b/r} \left[(\mu\delta + \delta^2/2)^l - (-\mu\delta + \delta^2/2)^l \right], \\ \mu\delta &= \sum_{l=1}^{\infty} \tfrac{1}{2} C_l^{r/b} \left[(\bar{\mu}\bar{\delta} + \bar{\delta}^2/2)^l - (-\bar{\mu}\bar{\delta} + \bar{\delta}^2/2)^l \right]. \end{aligned} \tag{18}$$

The emergent evolution (9) on the entire domain is derived with errors $\mathcal{O}(\delta^6)$. To obtain the same order of accuracy from the patch scheme we choose cutoff $\Gamma = 2$ in the coupling conditions (15) and we require up to $l = 4$ in the infinite sums in identities (16)–(18).

4.4 A patch scheme for two spatial dimensions

We now summarise the patch scheme that underlies Figure 1 for two dimensional heterogeneous diffusion. The aim is to show that the one dimensional case is readily generalisable to higher dimensions. We do not analyse the errors of the two dimensional scheme.

Let a two dimensional microscale lattice in the xy-plane be indexed by (i, j) and with some microscale field $u_{i,j}(t)$. Discretised diffusion on the 2D lattice with spacing h in both directions is then described by the system of ODEs

$$\begin{aligned}\dot{u}_{i,j}(t) = {} & \kappa^x_{i,j}[u_{i+1,j}(t) - u_{i,j}(t)]/h^2 + \kappa^x_{i-1,j}[u_{i-1,j}(t) - u_{i,j}(t)]/h^2 \\ & + \kappa^y_{i,j}[u_{i,j+1}(t) - u_{i,j}(t)]/h^2 + \kappa^y_{i,j-1}[u_{i,j-1}(t) - u_{i,j}(t)]/h^2\,, \end{aligned} \tag{19}$$

where diffusivity $\kappa^x_{i,j}$ is at half lattice point $(i + 1/2, j)$ and diffusivity $\kappa^y_{i,j}$ is at half lattice point $(i, j + 1/2)$. Define the heterogeneous diffusivity values to be K-periodic in the x-direction and L-periodic in the y-direction, then all diffusivities are contained in two $K \times L$ matrices called κ^x and κ^y. For example, Figure 1 with microscale periodicities $K = 2$ and $L = 4$ uses

$$\kappa^x = \begin{bmatrix} 3.16 & 1.39 & 0.10 & 0.22 \\ 2.40 & 1.34 & 3.28 & 0.83 \end{bmatrix}, \quad \kappa^y = \begin{bmatrix} 2.49 & 3.72 & 1.46 & 2.50 \\ 1.76 & 3.95 & 0.08 & 2.21 \end{bmatrix}. \tag{20}$$

The 2D macroscale lattice is indexed by (I, J), so the macroscale field values are denoted $U_{I,J}(t)$, and the lattice has spacing H in both directions. We construct rectangular patches of the microscale lattice with half-widths m and n lattice points centred on the macroscale coordinates (X_I, Y_J). When solving the system (19) only within these patches, we cater for the case of an ensemble of configurations to ensure the symmetry of the original microscale system (19) is maintained. In general there are $4KL$ configurations which include all reflections and translations of the diffusivities in κ^x and κ^y (if $K = 2, 3$ or $L = 2, 3$, then half these configurations are not unique). To consider only one configuration, rather than an entire ensemble, one would restrict equation (21) to $\ell = 1$. The discrete diffusion equation on patch (I, J) with configuration ℓ is, for $|i| \le (m-1)$, $|j| \le (n-1)$, and $\ell = 1, 2, \ldots, 4KL$,

$$\begin{aligned}\dot{u}_{(I,J),(i,j),\ell}(t) = {} & \kappa^x_{(i,j),\ell}[u_{(I,J),(i+1,j),\ell}(t) - u_{(I,J),(i,j),\ell}(t)]/h^2 \\ & + \kappa^x_{(i-1,j),\ell}[u_{(I,J),(i-1,j),\ell}(t) - u_{(I,J),(i,j),\ell}(t)]/h^2 \\ & + \kappa^y_{(i,j),\ell}[u_{(I,J),(i,j+1),\ell}(t) - u_{(I,J),(i,j),\ell}(t)]/h^2 \\ & + \kappa^y_{(i,j-1),\ell}[u_{(I,J),(i,j-1),\ell}(t) - u_{(I,J),(i,j),\ell}(t)]/h^2\,. \end{aligned} \tag{21}$$

The diffusion system (19) and its patch approximation (21) are the 2D equivalents of the 1D diffusion model (1) and its patch approximation (12).

Sections 4.2 and 4.3 define macroscale fields and coupling conditions for the 1D case; the 2D case is analogous, but here we only describe the $c = 0$ case and use ensemble averaging to smooth the microscale jaggedness. We define

the 2D macroscale field at (I, J) to be the ensemble average of the microscale values at the centre of the (I, J) patch:

$$U_{I,J} := \langle u_{(I,J),(0,0),\ell} \rangle. \tag{22}$$

We want the inter-patch coupling to express classic interpolation of these macroscale values $U_{I,J}$ to all the edges of each patch. Thus for the coupling conditions we invoke macroscale mean $\bar{\mu}_z$ and difference operators $\bar{\delta}_z$, with $z = x, y$ denoting the direction. Then interpolation determines the microscale field values along all four edges of each patch, for each configuration ℓ, are

$$\begin{aligned} u_{(I,J),(i,j),\ell} = U_{I,J} + \sum_{k+l>0}^{k+l\le\Gamma} \left\{ \prod_{p=0}^{k-1} \left[\left(\tfrac{ih}{H}\right)^2 - p^2 \right] \right\} \left\{ \prod_{p=0}^{l-1} \left[\left(\tfrac{jh}{H}\right)^2 - p^2 \right] \right\} \\ \times \gamma^{k+l} \frac{\left[\frac{2kH}{ih}\bar{\mu}_x \bar{\delta}_x^{2k-1} + \bar{\delta}_x^{2k}\right] \left[\frac{2lH}{jh}\bar{\mu}_y \bar{\delta}_y^{2l-1} + \bar{\delta}_y^{2l}\right]}{(2k)!(2l)!} U_{I,J} + \mathcal{O}(\gamma^{\Gamma+1}), \end{aligned} \tag{23}$$

where: either $i = \pm m$ for all $|j| \le n$ determining the left and right edges of the patch; or $j = \pm n$ for all $|i| \le m$ determining the top and bottom edges of the patch.

Equations (21)–(23) form a well-posed patch scheme provided some suitable macroscale boundary conditions are specified. Figure 1 is computed with the macroscale being doubly periodic.

The demonstration of Figure 1(top) uses a microscale 96×96 lattice to simulate the heterogeneous diffusion system (19) with doubly periodic boundary conditions, and initial condition $u_{i,j}(0) = 2\sin(\pi j/48)\cos(\pi i/48)$. With the microscale heterogeneous diffusivities (20), the system evolves after nondimensional time 0.5 to the black mesh in the figure showing the non-smooth effects of the heterogeneity. Figure 1(top) also superimposes the patch scheme prediction (shaded patches) obtained from just one configuration. For the patch scheme we use macroscale lattice of 6×6 square patches of half-widths $m, n = 4$. The patch fields are coupled by the interpolation (23) with truncation $\Gamma = 2$ which gives errors $\mathcal{O}(H^4)$ in the macroscale spacing. Figure 1(bottom) plots the patch scheme for the case when the coupling uses an ensemble average. The two component plots illustrate the difference between a patch scheme using a single diffusivity configuration and one using an ensemble average: the former captures heterogeneous structures, whereas the latter is smooth.

5 Optimise the patch parameters

We analytically test and optimise the design of the patch scheme by comparing the macroscale emergent evolution for a microsimulation over the entire domain, derived in Section 3, with the macroscale emergent evolution of the patch schemes. We determine the optimum patch parameters, defined by patch half-width n and core half-width c, for a given period K. Section 5.1 discusses how the error in the patch scheme evolution is measured.

Section 5.2 discusses the case where the microscale period K is known. In this case, choosing patch parameters n and c so that $K|(n-c)$ (that is, $K|b$) results in the scheme's emergent macroscale evolution to be correct to any given order of the coupling parameter γ. When $K|b$ then symmetries of the original entire domain are not corrupted by the imposition of patches, and thus there is also no need for an ensemble average.

Another good case is $K|(2c+1)$, which produces smaller errors in the patch scheme, when compared to most arbitrary choices of c, but this case still requires an ensemble average.

There are situations where we cannot design patches such that $K|b$ or $K|(2c+1)$. Two examples are when the microscale period $K > n$, or when the period K is unknown or not constant. Section 5.3 considers the optimum core half-width c for a given patch half-width n for a range of microscale diffusivity periods K and finds that good choices generally have the core half-width satisfying $n/3 \leq c \leq n/2$.

5.1 Assessing error in the patch scheme

This subsection determines the emergent macroscale behaviour of the patch schemes analogous to the analysis of Section 3.

The dynamic variables in the patch schemes are the field values in each patch for each configuration. Gather the variables in the jth patch as the vector $\mathbf{u}_j(t) = (u_{j,-n,1}, \ldots, u_{j,n,1}, \ldots, u_{j,-n,2K}, \ldots, u_{j,n,2K})$. Then abstractly, the patch schemes are in the differential-algebraic-operator form $\mathcal{B}\dot{\mathbf{u}}_j = \mathcal{A}\mathbf{u}_j/h^2$ for $(2n+1)2K \times (2n+1)2K$ operator-matrices $\mathcal{A}$ and $\mathcal{B}$. These operator-matrices are complicated and so are coded into computer algebra [3, Ancillary file `variD`].[1]

[1] We use the computer algebra package Reduce [http://reduce-algebra.com/] because it is both free and perhaps the fastest general purpose computer algebra system [9].

For example, we record here the simple case of one configuration, $\ell = 1$, microscale periodicity $K = 2$, and patch and core half-widths of $n = 4$ and $c = 1$ (so buffer width $b = n - c = 3$). Then $\mathcal{B} = \operatorname{diag}(0, 1, \dots, 1, 0)$ and the right-hand side matrix-operator, in terms of the arithmetic average $\bar{\kappa} = (\kappa_1 + \kappa_2)/2$,

$$\mathcal{A} = \begin{bmatrix} -\frac{1}{3} & -\frac{1}{3} & -\frac{1}{3} & \frac{1}{3}\varepsilon^{-3} & \frac{1}{3}\varepsilon^{-3} & \frac{1}{3}\varepsilon^{-3} & & & \\ \kappa_1 & -2\bar{\kappa} & \kappa_2 & & & & & & \\ & \kappa_2 & -2\bar{\kappa} & \kappa_1 & & & & & \\ & & \kappa_1 & -2\bar{\kappa} & \kappa_2 & & & & \\ & & & \kappa_2 & -2\bar{\kappa} & \kappa_1 & & & \\ & & & & \kappa_1 & -2\bar{\kappa} & \kappa_2 & & \\ & & & & & \kappa_2 & -2\bar{\kappa} & \kappa_1 & \\ & & & & & & \kappa_1 & -2\bar{\kappa} & \kappa_2 \\ & & & \frac{1}{3}\bar{\varepsilon}^3 & \frac{1}{3}\bar{\varepsilon}^3 & \frac{1}{3}\bar{\varepsilon}^3 & -\frac{1}{3} & -\frac{1}{3} & -\frac{1}{3} \end{bmatrix}.$$

The interior rows of $\mathcal{A}$ code the microscale ODEs (12), whereas the first and last rows code the inter-patch coupling conditions (14). The microscale shift operator ε is in turn expressed in terms of the γ-moderated macroscale mean and difference operators, $\bar{\mu}$ and $\bar{\delta}$ as used in (15), to code the coupling between the patches on an indefinitely sized macroscale domain.

Section 3 assumes the emergent solution $\mathbf{u} \sim e^{\lambda_1 t/h^2}\boldsymbol{v}_1$ for the dissipative system $\dot{\mathbf{u}} = M\mathbf{u}/h^2$ where λ_1 is the smallest real-part eigenvalue of matrix M; then λ_1 is evaluated assuming small wavenumber kh to describe the emergent macroscale evolution $\dot{U} = \lambda_1 U/h^2$ (9). Analogous to Section 3 we now seek the emergent solution of $\mathcal{B}\dot{\mathbf{u}}_j = \mathcal{A}\mathbf{u}_j/h^2$. This leads to the generalised eigenproblem $\lambda^{\text{pat}}\mathcal{B}\boldsymbol{v} = \mathcal{A}\boldsymbol{v}$ of which we want the leading operator-eigenvalue λ_1^{pat} as it characterises the emergent dynamics of the patch scheme, $\mathbf{u}_j \sim e^{\lambda_1^{\text{pat}} t/h^2}\boldsymbol{v}_1$ for $\boldsymbol{v}_1$ the eigenvector of λ_1^{pat}. In the small wavenumber kh limit the emergent macroscale dynamics of the patch scheme is $\dot{U} = \lambda_1^{\text{pat}} U/h^2$.

For the constructed $(2n+1)2K \times (2n+1)2K$ operator-matrices $\mathcal{A}$ and $\mathcal{B}$ the computer algebra code [3, Ancillary file `variD`] iteratively solves $\mathcal{B}\dot{\mathbf{u}}_j = \mathcal{B}g = \mathcal{A}\mathbf{u}_j$ for $\mathbf{u}_j$ and g. The initial values of $\mathbf{u}_j = (1, 1, \dots, 1)$ and constant g ensure we converge to the slowest solution $\mathbf{u}_j = \boldsymbol{v}_1$ and $g = \lambda_1^{\text{pat}}\mathbf{u}_j$. The computer algebra is limited by the combinatorial explosion in the diffusivity values $\kappa_1, \dots, \kappa_K$, even when restricted to moderate heterogeneity, and so we restrict the analysis to the diffusivity period range $2 \le K \le 12$ with patch half-width range $2 \le n \le 12$ and core half-widths $0 \le c < n$. The computer algebra code continues to iteratively improve g and $\mathbf{u}_j$ until they *exactly* satisfy the required matrix equation, up to chosen errors in diffusivity variations η and

coupling parameter γ (γ enters the problem via the shift operator ε). To compare λ_1^{pat} with λ_1 in (10) we accept errors in g and u_j of $\mathcal{O}(\delta^6, \eta^3)$, or equivalently $\mathcal{O}(\gamma^3, \eta^3)$. For the cases considered here, convergence typically requires five or six iterations, and always fewer than nine. The computer algebra determines g in terms of macroscale operators $\bar{\delta}$ and $\bar{\mu}$ so we apply equations (16) and (18) to obtain g in terms microscale operators δ and μ, thus facilitating the comparison of λ_1^{pat} with λ_1.

The form of the asymptotic approximations for λ_1^{pat} in the patch scheme obtained from computer algebra is the same as equation (10), but typically with different coefficients which we denote by d^{pat}, d_k^{pat} and f_k^{pat}. To find the best performing patch parameters we mainly explore quadratic effects in the relative diffusivity variations η_i of the second difference term, δ^2, characterised by the quadratic coefficients d_k in the relative diffusivities. Such quadratic terms include the effects of physical correlations in the microscale structure that may be significant in applications (the $\eta_i\eta_{i+k}$ terms in (10)). To compare the macroscale emergent evolution from (10) with that of a patch scheme we compare relative errors in the quadratic coefficients d_k of the leading eigenvalue λ_1, namely the relative error

$$\rho_k := \left| \frac{d_k - d_k^{\text{pat}}}{d_k} \right| \quad \text{for } k = 0, 1, \ldots, K/2\,. \tag{24}$$

For example, for microscale period $K = 3$, patch half-width $n = 7$, and core half-width $c = 3$, the computer algebra code [3] converges after five iterations and determines the coefficients

$$d^{\text{pat}} = \frac{1}{3}\,, \quad d_0^{\text{pat}}, d_1^{\text{pat}} = \frac{12541}{56448} \approx 0.22\,, \quad f_0^{\text{pat}}, -f_1^{\text{pat}} = \frac{71}{896} \approx 0.08\,. \tag{25}$$

From the full microscale derivation of the coefficients (11), the δ^2 coefficients are $d = \frac{1}{3}$ and $d_0, d_1 = \frac{2}{9}$ whereas the δ^4 coefficients are $f_0, -f_1 = \frac{2}{27}$. In this case, the δ^2 coefficients have relative errors of $\rho_0, \rho_1 = 2.4 \times 10^{-4}$. A similar calculation for the δ^4 coefficients f_0 and f_1 reveals a larger relative error of 7.0×10^{-2}. For the same patch and core half-widths but a microscale period of $K = 7$, convergence is again obtained after five iterations and gives coefficients

$$\begin{aligned} &d^{\text{pat}} = \frac{1}{7}\,, \quad d_0^{\text{pat}} = \frac{6}{49}\,, \quad d_{1,2,3}^{\text{pat}} = \frac{2}{49}\,, \quad f_0^{\text{pat}} = \frac{81}{784}\,, \\ &f_1^{\text{pat}} = \frac{207}{3136}\,, \quad f_2^{\text{pat}} = -\frac{157}{3136}\,, \quad f_3^{\text{pat}} = -\frac{187}{1568}\,, \end{aligned} \tag{26}$$

and, from equation (11), the δ^2 coefficients are $d = \frac{1}{7}$, $d_0 = \frac{6}{49}$ and $d_{1,2,3} = \frac{2}{49}$ and the δ^4 coefficients are $f_0, -f_3 = \frac{4}{49}$ and $f_1, -f_2 = \frac{2}{49}$. In this case the patch dynamics scheme obtains the exact δ^2 coefficients, but the δ^4 coefficients have large relative errors between 0.23 and 0.62.

The next subsections aim to determine what patch parameters n and c minimise the relative error ρ_k. We consider a range of microscale periods K and draw general conclusions about the best choices of n and c.

5.2 Ideal patch parameters give the correct macroscale

In the case when the microscale period K exactly divides the difference between the patch and core half-widths, $K|(n-c)$, or equivalently, the microscale period exactly divides the buffer width $K|b$, computer algebra [3] derives that $\lambda_1^{\text{pat}} = \lambda_1 + \mathcal{O}(\delta^6, \eta^3)$ for all $2 \le K \le 12$ and $2 \le n \le 12$. That is, in this case patch dynamics *exactly* reproduces the emergent macroscale λ_1 in equation (10), not only with the correct d_k coefficients ($\rho_k = 0$) but also the correct f_k coefficients. The correct coefficients are obtained even *without an ensemble average*, saving considerable computational expense[2]. Furthermore, for periods $K = 2$ and 3 with $K|b$, computer algebra derives that the equality $\lambda_1^{\text{pat}} = \lambda_1 + \mathcal{O}(\delta^6)$ holds for general diffusivities κ_i with no assumption that the heterogeneity be moderate[3]. That is, the patch scheme *exactly* reproduces the δ^2 and δ^4 terms characterised in equation (9). A combinatorial explosion of terms prevents the computer algebra from analysing microscale periods $K > 3$ with general diffusivities. Nonetheless, numerical simulations in Section 6 indicate that the condition $K|b$ gives the optimum patch design, for any microscale periodicity K, and for any variation in heterogeneity.

The numerical results suggest that the accuracy of the patch dynamics scheme is better than the algebraically determined $\lambda_1^{\text{pat}} = \lambda_1 + \mathcal{O}(\delta^6, \eta^3)$. However, the algebraic result is significant because it means that the patch scheme accurately captures the dependence of the macroscale evolution on the fine microscale detail, not just the homogenised characteristics. The second difference, δ^2, terms of equation (10) with error $\mathcal{O}(\delta^4, \eta^3)$ are directly expressible in terms of the geometric, harmonic and algebraic mean diffusivities. However, the

[2] In the computer algebra code [3] setting parameter `ens=2` preforms an ensemble average over $2K$ configurations whereas `ens=0` uses only one configuration.

[3] In the computer algebra code [3] `simplify=1` assumes moderate heterogeneity of an order determined by `eord`, and `simplify=0` assumes no heterogeneity. In the latter case, iterations continue until the matrix equation is correct to a chosen order of γ.

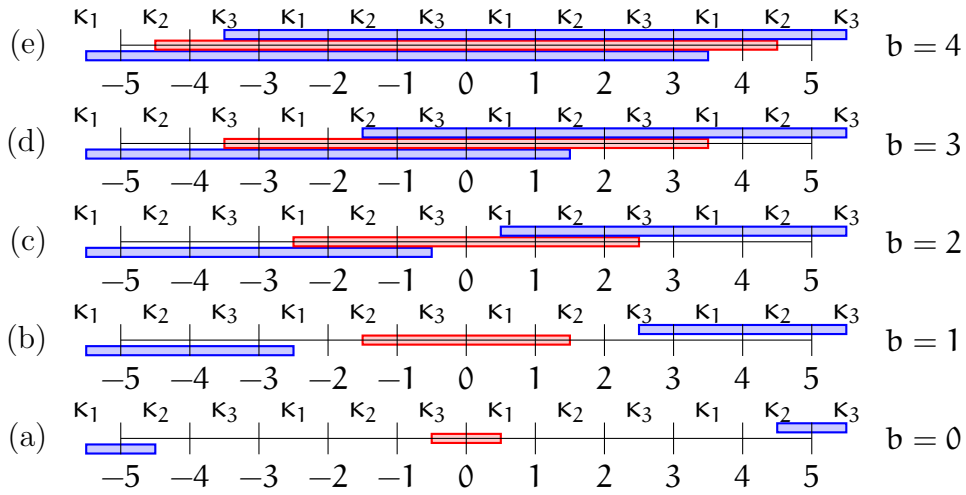

Figure 6: Microscale structure of a single patch with half-width $n = 5$, diffusivity period $K = 3$ and different core half-widths c. For each case, the core and action regions are indicated by the shaded outlined regions. When $c = 2$, $K|b$ is true (both buffers capture a multiple of a complete period of diffusivities) and only then do the two action regions and core capture the same diffusivity pattern: κ_1 to the left, κ_3 to the right and $\kappa_2, \kappa_3, \kappa_1, \kappa_2$ inside. When $c = (K-1)/2 = 1$ both action regions and core capture one complete diffusivity period, but not in the same order. Similarly, when $c = (3K-1)/2 = 4$ both action regions and core capture two complete diffusivity periods.

fourth difference, δ^4, terms depend upon the detailed microscale structure, such as the ordering of the diffusivities on the microscale grid. Thus, in accurately matching the coefficients f_k, the patch scheme provides an accurate macroscale closure of the microscale detail.

The patch scheme accurately predicts the macroscale evolution on the entire domain when $K|b$ because the patch system captures the crucial necessary symmetry of the original microscale system (1). Our construction of the coupling conditions (15) is reliant on a shift of $\pm b$ microscale lattice points of the microscale fields $u_{j,i,\ell}$ in the patch core where $|i| \le c$ to the microscale fields in the action regions where $(n-2c) \le \pm i \le n$, as illustrated in Figure 4. When $K|b$, the core and both action regions contain identical diffusivities in identical placement (illustrated in Figure 6(c) for the case $K = 3$ and $n = 5$). Further, when $K|b$ both buffers contain a multiple of a complete period. For $K|b$, the symmetry of the model is reflected in the patch via the symmetry of the action regions and core as well as both buffers.

As shown in Figure 6(b) and Figure 6(e), there are cases where the core and the action regions capture a multiple of a complete period of microscale structure, with one period captured in the former and two periods in the latter (although there is nothing notable about the buffer regions). In general this requires $K|(2c+1)$ so is only possible in our scheme when K is odd. For $K|(2c+1)$ computer algebra finds that the patch scheme eigenvalue λ_1^{pat} gives precisely the d_k coefficients in the macroscale evolution λ_1 (10); that is, the relative error $\rho_k = 0$ for all k. However, generally this precise modelling does not hold without an ensemble average or for large variation in diffusivities. Unlike the case $K|b$, in the case $K|(2c+1)$ the patch scheme only approximates the δ^4 coefficients f_k. The last example in Section 5.1 with $n = 7$, $c = 3$ and $K = 7$ satisfies $K|(2c+1)$ and the d_k^{pat} coefficients in (26) are identical to d_k; however, the f_k^{pat} coefficients are not particularly accurate when compared to f_k. For even K, and when using an ensemble average of moderately varying diffusivities, although we cannot fit a multiple of diffusivity periods into the core or action regions, we do tend to find that the relative error ρ_k is relatively small for all k when $K|2c$ or $K|2(c+1)$.

In general, when implementing a patch scheme, if we know the microscale period K and are free to choose any patch parameters, then we should choose patch half-width n and action and core half-widths c such that $K|(n-c)$ ($K|b$) since the scheme, with only one configuration, accurately simulates the emergent macroscale evolution. For large period K, if we only require δ^2 accuracy, then choosing c such that $K|(2c+1)$ might appear to be a better choice since it holds for smaller patch sizes $(K-1)/2 < n$, but this case requires an ensemble average, which also becomes computationally expensive as K becomes large, albeit parallelisable.

5.3 Optimum patch parameters when uncertain

In some applications we will not necessarily know the microscale period K, perhaps because there is no well-defined period as in an agent/particle based simulation. This section explores the patch dynamics evolution λ_1^{pat} when the ideal patch parameters satisfying $K|b$ are not knowable. We seek patch parameters which are independent of the unknown period K and minimise the relative error ρ_k in the second order coefficients d_k in the ensemble averaged patch dynamics evolution λ_1^{pat} of the macroscale evolution (10). We find that the general behaviour of the relative error ρ_k is both qualitatively and quantitatively similar for all k, so here only present ρ_0 which measures the accuracy of d_0.

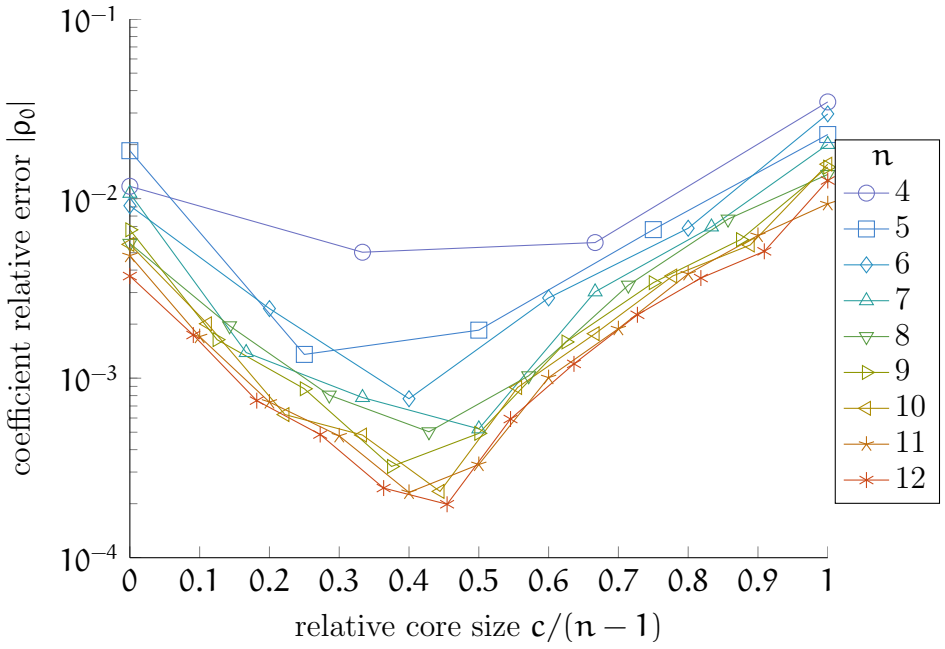

Figure 7: Coefficient relative error $|\rho_0|$ averaged over microscale periodicities $2 \le K \le n$ versus the relative core half-width $0 \le c/(n-1) \le 1$ for patch sizes $4 \le n \le 12$. The coefficient error $|\rho_0|$ is minimised when $c \approx 0.4n$.

Figure 7 plots the relative errors $|\rho_0|$ of d_0^{pat} coefficients calculated from computer algebra [3] compared to d_0 in equation (11). These relative errors are calculated for various patch and core half-widths, n and c and averaged over all $2 \le K \le n$. This figure caters for microscale periods which fit within half a patch. The worst choices are the smallest and largest possible core half-widths $c = 0, (n-1)$. The relative error $|\rho_0|$ is minimised by $c \approx 0.4n$. In general, $n/3 \le c \le n/2$ produces the most accurate solutions for a given patch half-width n. Section 5.1 considered the case $n = 7$, $c = 3$ and $K = 3$, with coefficients presented in equation (25). This example is typical of cases with $c \approx 0.4n$ since errors $\rho_k \sim 2 \times 10^{-4}$ are quite small. This example also calculates errors of about 7×10^{-2} for the f_k^{pat} coefficients compared to f_k, which are significantly larger than ρ_k, but are not unreasonably large.

Figure 7 also shows that the relative error decreases with increasing patch size n, keeping $c/(n-1)$ fixed. Thus larger patches generally give more accuracy, albeit at the expense of more microscale computation.

Figure 8 again plots the relative error $|\rho_0|$ of d_0^{pat} coefficients calculated from computer algebra [3] compared to d_0 in equation (11), but now the error is

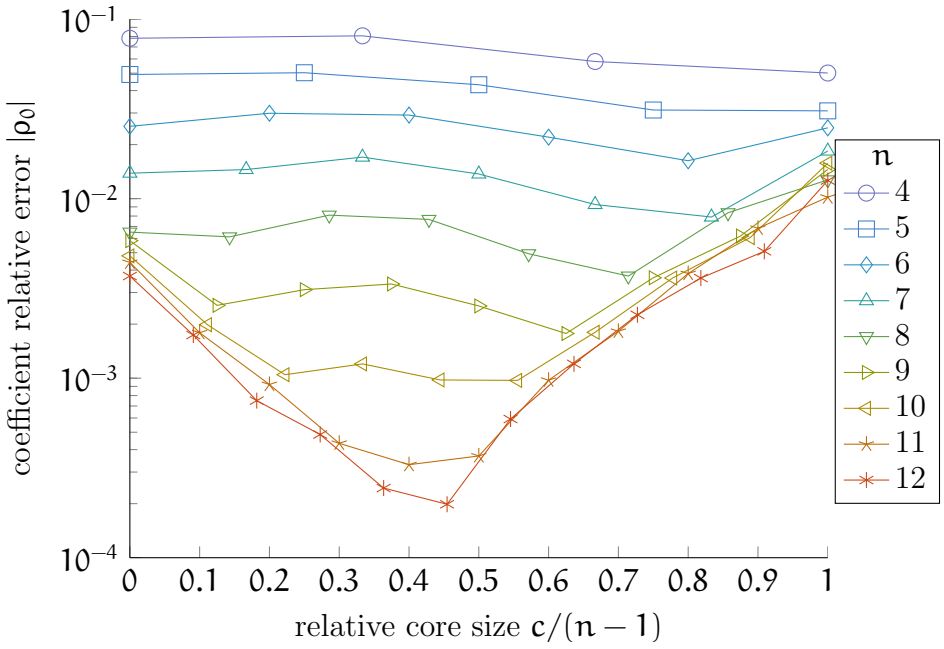

Figure 8: Coefficient relative errors $|\rho_0|$ averaged over microscale periods $2 \le K \le 12$, including cases $K > n$, versus the relative core half-width $0 \le c/(n-1) \le 1$ for patch sizes $4 \le n \le 12$. The coefficient error $|\rho_0|$ is minimised when $c \approx 0.4n$ for large n, but as n decreases the minima are less clear.

averaged over a larger range of microscale periods, namely $2 \le K \le 12$. This average includes large microscale periods which do not fit within one patch. When most periods do not fit within one patch, as is the case for small n, the error $|\rho_0|$ is rather large with a slight minimum near the largest core half-width $c \approx n-1$. As the patch size n increases, the minimum become sharper as the patch is better able to accommodate all K diffusivities in the range $2 \le K \le 12$. The position of the minimum also shifts to smaller core sizes c and approaches $c \approx 0.4n$ as n increases.

Figure 8 indicates that the patch scheme does not accurately predict the macroscale evolution when the period of significant microscale structure K is significantly larger than the patch half-width n, with errors in the second order coefficients up to 10%. Nonetheless, with ensemble averaging, the patch scheme does precisely model the mean diffusivity of small microscale heterogeneity (the linear coefficient d in (10)).

6 Numerical simulations

This section compares numerical simulations of the original entire domain diffusion problem (1) with simulations of the patch scheme (12) with the patch coupling conditions (15). These simulations provide additional evidence for claims in Section 5 regarding optimum choices of patch half-width n and core half-width c. In this section we choose diffusivities with large microscale variations to test the patch scheme outside the domain addressable by the algebraic results of Section 5.

Using computer algebra, Section 5.2 found that, provided $K|b$, $\lambda_1^{\text{pat}} = \lambda_1 + \mathcal{O}(\delta^6, \eta^3)$ and for $K = 2, 3$, again provided $K|b$, we need not assume any microscale heterogeneity and $\lambda_1^{\text{pat}} = \lambda_1 + \mathcal{O}(\delta^6)$. These orders of error are not determined from limitations in the patch dynamics scheme but from computer algebra limitations (in the case of $\mathcal{O}(\eta^3)$) and from our analytic derivation of λ_1 in Section 3 (in the case of $\mathcal{O}(\delta^6)$). Here, with numerical simulations, we avoid the limitations imposed by the algebraic derivations and determine the error in the patch scheme for optimal patch parameter satisfying $K|b$. We find that the error of the patch dynamics scheme is determined by the coupling order Γ which defines the order of γ truncations in the coupling conditions (15).

We numerically solve the diffusion system (1) on the entire domain with macroscale periodic boundary conditions and a domain of length 20 containing 192 lattice points, so lattice spacing $h = 0.1042$. We choose initial condition $u_i(0) = 2\sin(\pi i/96)$ for $i = 0, \ldots, 191$ to investigate only the smallest magnitude nonzero eigenvalue (on the λ_1 branch) varying slowly across space. We randomly select 12 different diffusivity structures, half with $K = 4$ and half with $K = 6$, and all with harmonic mean $\kappa = 1$. The randomly chosen diffusivities have log-normal distributions where the standard deviation of the log is 4. Diffusivities are then scaled to have harmonic mean $\kappa = 1$. For each diffusivity structure we consider a different set of patch parameters. For $K = 4$ we set $(n, c) = (4, 0), (5, 1), (6, 2), (7, 3), (8, 4), (8, 0)$, so that we always have $K|(n - c)$. For $K = 6$ we set $(n, c) = (6, 0), \ldots, (11, 5)$, again ensuring $K|(n - c)$. We solve the 12 problems with the patch scheme, without an ensemble average, using macroscale lattice spacing $H = 24h = 2.5$ so that there are eight equally spaced patches across the domain.

To compare the entire domain solution $u_i(t)$ and the patch scheme's $u_{j,i}(t)$ we calculate the relative error of the patch scheme $|[u_i - u_{j,0}]/u_i|$ at the centre of each patch, so $i = 24j - 12$. Over the time period $0 \le t \le 5$ we find that the error increases linearly with time in all patches j so we

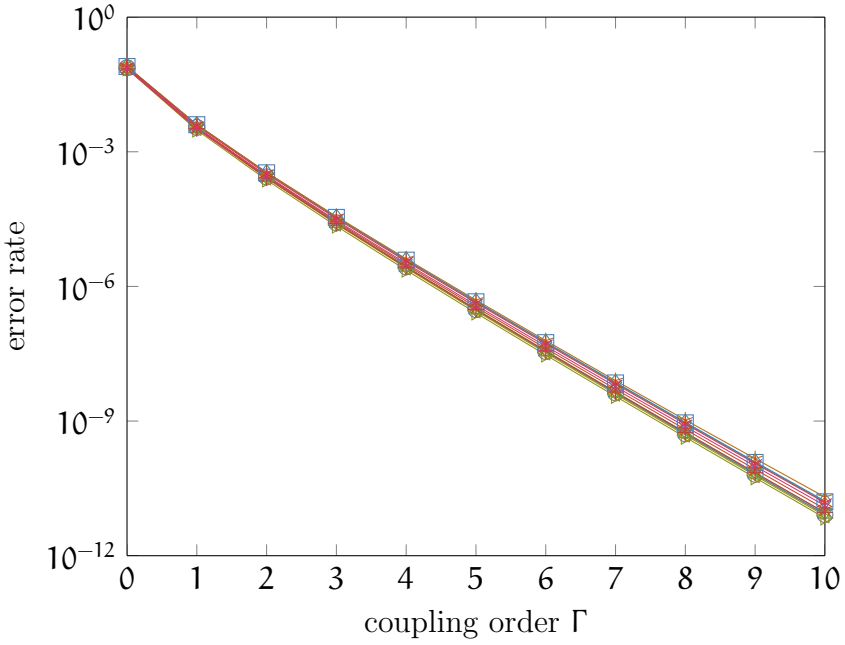

Figure 9: Rate of error increase per unit time in the patch scheme versus order of the coupling Γ for 12 different, randomly chosen, diffusivity configurations with log-normal distributions and standard deviation of the log 4. All diffusivity configurations are scaled to harmonic mean $\kappa = 1$. The error is measured relative to the entire domain solution, for patch half-widths n and core half-widths c constrained by $K|b$. The error decreases exponentially with coupling order Γ and there is little to distinguish the 12 different plots, except for some slight differences at high order.

calculate the rate of maximum error increase for all j per unit time. Figure 9 plots this rate of maximum error growth versus the order of coupling Γ in the coupling conditions (15). The error in the patch scheme decreases exponentially with order Γ and there is little to distinguish the 12 different diffusivity configurations. Although Figure 9 indicates that the patch scheme error can be made as small as we like, as in any spatial discretisation we expect stability considerations to limit the patch scheme to small values of Γ for more general microscale systems. Furthermore, very large coupling orders are numerically expensive because they limit parallelisation of code. Therefore, in most patch dynamics simulations we expect a coupling order of approximately $2 \leq \Gamma \leq 5$ to be most suitable.

Section 5.3 claims that for unknown periodicity K the patch scheme with an ensemble average is best performed with larger patch half-width n and a

core half-width satisfying $n/3 \leq c \leq n/2$. Numerical simulations (not shown here) were performed over a range of different periodicities and diffusivity configurations, including large diffusivity variations (not moderate). Numerical results support the recommendation of $n/3 \leq c \leq n/2$ with n as large as practically computable.

7 Conclusion

By analysing the emergent, macroscale, evolution we established that the patch scheme for multiscale modelling captures the macroscale emergent dynamics of a microscale heterogeneous lattice systems. For best results it is important to appropriately choose the patch parameters, defined by the patch half-width n and the core half-width c, relative to the underlying period K of the microscale detail. Other microscale systems with heterogeneous microscale require similar consideration when implementing the patch scheme.

For the heterogeneous diffusion system considered here, the the patch scheme's error is minimised by choosing patch and core half-widths, n and c, such that microscale period $K|(n-c)$; that is, $K|b$ in terms of the buffer width. The buffer plays an important role in patch dynamics, providing space for the solution to evolve from the imposed coupling conditions to a more exact solution in the centre of the patch. For a choice of patch and core (or buffer size) such that $K|b$, not only is the entire domain evolution accurately obtained by patch dynamics, but the computational time is reduced by, without loss of accuracy, considering only one configuration rather than an ensemble average. Our results are supported by both algebra and numerical calculations.

When, for whatever reason, $K|b$ cannot be known to be satisfied, we choose $n/3 \leq c \leq n/2$ and rely on an ensemble average to maintain the symmetry of the original microscale problem. In this case the accuracy of the results depend on the extent of the variability in the diffusivities and the patch half-width n, with larger n generally producing more accurate results.

The microscale dynamics considered is left-right symmetric, since we only describe diffusion and not advection in the original microscale system. We used this symmetry property to construct an ensemble of $2K$ configurations, K translations and K reflections of the original diffusivity configuration. Future work will consider patch dynamics for multiscale modelling of microscale advection-diffusion equations, in both one and two dimensions. The presence of advection terms will require a reconsideration of the ensemble. We expect

that the patch geometry which best describes the emergent macroscale dynamics will complement any underlying symmetry of the detailed microscale problem.

Our analysis on the one dimensional, microscale heterogeneous, lattice diffusion system (1) is readily applicable to other systems. For example, if the temporal derivative $\dot{u}_i$ in system (1) is replaced with a second derivative $\ddot{u}_i$, we then form a one dimensional lattice wave equation where κ_i is a K periodic, microscale heterogeneity in the wave system. In physical problems, small unmodelled damping will eliminate the high frequency modes and the macroscale modes are the remaining low frequency modes. Then the macroscale dynamics is still characterised by the smallest magnitude eigenvalue λ_1 since solutions are of the form $u_i \sim e^{\sqrt{\lambda_1}t/h}$. Thus the low frequency, long wave, macroscale model will be of the form $\ddot{U}_j = \lambda_1 U_j/h^2$ for exactly the same operator eigenvalues λ_1 and λ_1^{pat} explored here. Consequently our results on the design of a patch scheme also apply to waves in analogous heterogeneous media.

Acknowledgements The Australian Research Council Discovery Project grants DP0988738 and DP120104260 helped support this research.

References

[1] B. Aulbach and T. Wanner. The Hartman–Grossman theorem for Caratheodory-type differential equations in Banach spaces. *Nonlinear Anal.: Theor.*, 40(1–8):91–104, 2000. doi:10.1016/S0362-546X(00)85006-3.

[2] J. E. Bunder and A. J. Roberts. Patch dynamics for macroscale modelling in one dimension. In M. I. Nelson, A. J. Roberts, M. Coupland, T. J. Hamilton, and H. S. Sidhu, editors, *Proceedings of the 10th Biennial Engineering Mathematics and Applications Conference (EMAC2011)*, volume 53 of *ANZIAM J.*, pages C280–C295, 2012. http://journal.austms.org.au/ojs/index.php/ANZIAMJ/article/view/5074.

[3] J. E. Bunder, A. J. Roberts, and I. G. Kevrekidis. Better buffers for patches in macroscale simulation of systems with microscale randomness. Technical Report, 2013. http://arxiv.org/abs/1312.1415.

[4] D. N. Cheban. *Global Attractors of Non-Autonomous Dissipative Dynamical Systems*, volume 1 of *Interdisciplinary Mathematical Sciences*. World Scientific, 2004. doi:10.1142/5643.

[5] J. Chu, B. Engquist, M. Prodanovic, and R. Tsai. A multiscale method coupling network and continuum models in porous media i: Steady-state single phase flow. *Multiscale Model. Sim.*, 10(2):515–549, 2012. doi:10.1137/110836201.

[6] J. O. Dada and P. Mendes. Multi-scale modelling and simulation in systems biology. *Integr. Biol.*, 3:86–96, 2011. doi:10.1039/C0IB00075B.

[7] A. Degenhard and J. Rodríguez-Laguna. Renormalization group methods for coarse-graining of evolution equations. In A. N. Gorban, I. G. Kevrekidis, C. Theodoropoulos, N. K. Kazantzis, and H. C. Öttinger, editors, *Model Reduction and Coarse-Graining Approaches for Multiscale Phenomena*, pages 177–206. Springer, 2006. doi:10.1007/3-540-35888-9_8.

[8] J. Dolbow, M. A. Khaleel, J. Mitchell, Pacific Northwest National Laboratory (U.S.), and United States. Dept. of Energy. *Multiscale Mathematics Initiative: A Roadmap*. Pacific Northwest National Laboratory, 2004. `http://science.energy.gov/~/media/ascr/pdf/research/am/docs/Multiscale_math_workshop_3.pdf`.

[9] R. Fateman. Comparing the speed of programs for sparse polynomial multiplication. *ACM SIGSAM Bull.*, 37(1):4–15, Mar. 2003. doi:10.1145/844076.844080.

[10] M. Fermeglia and S. Pricl. Multiscale molecular modeling in nanostructured material design and process system engineering. *Comput. Chem. Eng.*, 33(10):1701–1710, 2009. doi:10.1016/j.compchemeng.2009.04.006.

[11] D. Givon, R. Kupferman, and A. Stuart. Extracting macroscopic dynamics: model problems and algorithms. *Nonlinearity*, 17(6):R55, 2004. doi:10.1088/0951-7715/17/6/R01.

[12] I. G. Goryacheva. Multiscale modelling in contact mechanics. In F. M. Borodich, editor, *IUTAM Symposium on Scaling in Solid Mechanics*, volume 10 of *Iutam Bookseries*, pages 123–134. Springer, 2009. doi:10.1007/978-1-4020-9033-2_12.

[13] M. F. Horstemeyer. *Practical Aspects of Computational Chemistry: Methods, Concepts and Applications*, chapter Multiscale Modeling: A Review, pages 87–135. Springer, 2010. doi:10.1007/978-90-481-2687-3_4.

[14] G. Hütter, U. Mühlich, and M. Kuna. Micromorphic homogenization of a porous medium: elastic behavior and quasi-brittle damage. *Continuum Mechanics and Thermodynamics*, pages 1–14, 2014. doi:10.1007/s00161-014-0402-5.

[15] J. M. Hyman. Patch dynamics for multiscale problems. *Comput. Sci. Eng.*, 7(3):47–53, 2005. doi:10.1109/MCSE.2005.57.

[16] G. E. Kapellos and T. S. Alexiou. Modeling momentum and mass transport in cellular biological media: from the molecular to the tissue scar. In S. M. Becker and A. V. Kuznetsov, editors, *Transport in Biological Media*, pages 1–40. Elsevier, 2013. https://www.elsevier.com/books/transport-in-biological-media/becker/978-0-12-415824-5.

[17] I. G. Kevrekidis and G. Samaey. Equation-free multiscale computation: Algorithms and applications. *Annu. Rev. Phys. Chem.*, 60(1):321–344, 2009. doi:10.1146/annurev.physchem.59.032607.093610.

[18] S. Knapek. Matrix-dependent multigrid homogenization for diffusion problems. *SIAM J. Sci. Comput.*, 20(2):515–533, 1998. doi:10.1137/S1064827596304848.

[19] P. Ladeveze. Multiscale modelling and computational strategies for composites. *Int. J. Numer. Meth. Engng*, 60(1):233–253, 2004. doi:10.1002/nme.960.

[20] J. Li, P. Kevrekidis, C. Gear, and I. Kevrekidis. Deciding the nature of the coarse equation through microscopic simulations: The baby-bathwater scheme. *SIAM Rev.*, 49(3):469–487, 2007. doi:0.1137/070692303.

[21] C. C. Mei and B. Vernescu. *Homogenization Methods for Multiscale Mechanics*. World Scientific, 2010. doi:10.1142/7427.

[22] J. Möller, O. Runborg, P. G. Kevrekidis, K. Lust, and I. G. Kevrekidis. Equation-free, effective computation for discrete systems: a time stepper based approach. *Int. J. Bifurcat. Chaos*, 15(3):975–996, 2005. doi:10.1142/S0218127405012399.

[23] G. Pavliotis and A. Stuart. *Multiscale Methods: Averaging and Homogenization*. Springer, 2008. doi:10.1007/978-0-387-73829-1.

[24] G. A. Pavliotis and A. M. Stuart. *Multiscale methods: averaging and homogenization*, volume 53 of *Texts in Applied Mathematics*. Springer, 2008. doi:10.1007/978-0-387-73829-1.

[25] A. J. Roberts. Holistic discretization ensures fidelity to Burgers' equation. *Appl. Numer. Math.*, 37(3):371–396, 2001. doi:10.1016/S0168-9274(00)00053-2.

[26] A. J. Roberts. A holistic finite difference approach models linear dynamics consistently. *Math. Comput.*, 72:247–262, 2003. doi:10.1090/S0025-5718-02-01448-5.

[27] A. J. Roberts. *Model emergent dynamics in complex systems*. SIAM, 2015.

[28] A. J. Roberts and I. G. Kevrekidis. General tooth boundary conditions for equation free modeling. *SIAM J. Sci. Comput.*, 29(4):1495–1510, 2007. doi:10.1137/060654554.

[29] A. J. Roberts, T. MacKenzie, and J. E. Bunder. A dynamical systems approach to simulating macroscale spatial dynamics in multiple dimensions. *J. Eng. Math.*, 86(1):175–207, 2014. doi:10.1007/s10665-013-9653-6.

[30] O. Runborg, C. Theodoropoulos, and I. G. Kevrekidis. Effective bifurcation analysis: a time-stepper-based approach. *Nonlinearity*, 15(2):491–511, 2002. doi:10.1088/0951-7715/15/2/314.

[31] G. Samaey, I. G. Kevrekidis, and D. Roose. Patch dynamics with buffers for homogenization problems. *J. Comput. Phys.*, 213(1):264–287, 2006. doi:10.1016/j.jcp.2005.08.010.

[32] G. Samaey, A. J. Roberts, and I. G. Kevrekidis. Equation-free computation: an overview of patch dynamics. In J. Fish, editor, *Bridging the Scales in Science and Engineering*, pages 216–246. Oxford University Press, 2010. http://ukcatalogue.oup.com/product/9780199233854.do.

[33] G. Samaey, D. Roose, and I. G. Kevrekidis. Combining the gap-tooth scheme with projective integration: Patch dynamics. In B. Engquist, O. Runborg, and P. Lötstedt, editors, *Multiscale Methods in Science and Engineering*, volume 44 of *Lecture Notes in Computational Science and Engineering*, pages 225–239. Springer, 2005. doi:10.1007/3-540-26444-2_12.

[34] V. V. Silberschmidt. Account for random microstructure in multiscale models. In Y. W. Kwon, D. H. Allen, and R. Talreja, editors, *Multiscale Modeling and Simulation of Composite Materials and Structures*, pages 1–35. Springer, 2008. doi:10.1007/978-0-387-68556-4.

[35] N. I. Zheludev and Y. S. Kivshar. From metamaterials to metadevices. *Nature Mat.*, 11:917–924, 2012. doi:10.1038/nmat3431.